He-accreting WDs: AM CVn stars with WD donors

L. Piersanti,[1,2]★ L. R. Yungelson[3]★ and A. Tornambé[4]★

[1]*INAF-Osservatorio Astronomico di Teramo via Mentore Maggini, snc, I-64100, Teramo, Italya*
[2]*INFN-Sezione di Napoli, I-80126 Napoli, Italy*
[3]*Institute of Astronomy, Pyatnitskaya 48, 119017 Moscow, Russia*
[4]*INAF-Osservatorio Astronomico di Roma via di Frascati, 33, I-00040, Monte Porzio Catone, Italy*

ABSTRACT

We study the physical and evolutionary properties of the 'white dwarf (WD) family' of AM CVn stars by computing realistic models of interacting double-degenerate systems. We evaluate self-consistently both the mass-transfer rate from the donor, as determined by gravitational wave emission and interaction with the binary companion, and the thermal response of the accretor to mass deposition. We find that, after the onset of mass transfer, all the considered systems undergo a strong non-dynamical He-flash. However, due to the compactness of these systems, the expanding accretors fill their Roche lobe very soon, thus preventing the efficient heating of the external layers of the accreted CO WDs. Moreover, due to the loss of matter from the systems, the orbital separations enlarge and mass transfer comes to a halt. The further evolution depends on the value of $\dot{M}$ after the donors fill again their lobe. On one hand, if the accretion rate, as determined by the actual value of $(M_{\rm don}, M_{\rm acc})$, is high enough, the accretors experience several He-flashes of decreasing strength and then quiescent He-burning sets in. Later on, since the mass-transfer rate in IDD is a permanently decreasing function of time, accretors experience several recurrent strong flashes. On the other hand, for intermediate and low values of $\dot{M}$ the accretors enter directly the strong flashes accretion regime. As expected, in all the considered systems the last He-flash is the strongest one, even if the physical conditions suitable for a dynamical event are never attained. When the mass accretion rate decreases below $(2\text{--}3) \times 10^{-8}\,M_\odot\,\mathrm{yr}^{-1}$, the compressional heating of the He-shell becomes less efficient than the neutrino cooling, so that all the accretors in the considered systems evolve into massive degenerate objects. Our results suggest that SNe .Ia or Type Ia Supernovae due to Edge-Lit Detonation in the WD family of AM CVn stars should be much more rare than previously expected.

Key words: accretion, accretion discs – binaries: general – supernovae: general – white dwarfs.

1 INTRODUCTION

AM CVn stars are ultracompact cataclysmic binaries with spectra dominated by helium. At the time of writing this article, 43 confirmed and candidate objects were known [see table 1 in Levitan et al. (2015), and Wagner et al. 2014; Kato, Hambsch & Monard 2015. Measured orbital periods range from 5.5 to 65 min. There exist also several cataclysmic variables (some with hydrogen-deficient spectra) below the conventional minimum $P_{\rm orb}$ of CV (70–80) min., which may be AM CVn stars in making (Breedt et al. 2012; Carter et al. 2013b; Littlefield et al. 2013; Garnavich et al. 2014; Ramsay et al. 2014). The significance of AM CVn stars stems from their

importance for the studies of very late stages of evolution of binary stars and of accretion discs physics; moreover they are considered primary targets and verification sources for high-frequency gravitational waves detectors. The current models of AM CVn stars envision a semidetached binary harbouring a carbon–oxygen white dwarf (CO WD) accreting He-rich matter. The donor may be either a helium WD or a low-mass helium star or a core of a main-sequence star strongly evolved prior to Roche lobe overflow (RLOF). The evolution of AM CVn binaries is driven by angular momentum loss via gravitational waves radiation (GWR). An overview and a discussion of observational features, formation and evolution of these stars, as well as models for their discs, may be found, e.g. in Warner (2003), Nelemans (2005, 2009), Ruiter et al. (2010), Solheim (2010), Kotko et al. (2012), Amaro-Seoane et al. (2013), Postnov & Yungelson (2014), Cannizzo & Nelemans (2015). The

★ E-mail: piersanti@oa-teramo.inaf.it (LP); lev.yungelson@gmail.com (LRY); tornambe@oa-teramo.inaf.it (AT)

topic of the present study is AM CVn systems with WD donors, sometimes also called 'interacting double-degenerates' (IDD) or 'white-dwarf family of AM CVn stars'.

An essential issue defining the formation of AM CVn stars is the stability of mass transfer by degenerate donors (Tutukov & Yungelson 1979; Nelemans et al. 2001; Marsh, Nelemans & Steeghs 2004). In double-degenerate systems, Roche lobe is first filled by the lighter of two WDs (in the context of this section – the secondary with mass M_2). Since for WDs the power of the mass–radius relation is close to $-1/3$, systems with initial $q = M_2/M_1 > 2/3$ are dynamically unstable. The components separation a of nascent AM CVn's is so small that mass-exchange almost definitely begins in the direct-impact mode, without formation of the disc. Strict condition of stability for the case of no feedback of the angular momentum of the accreted material to the orbit becomes

$$q < 1 + (\xi_2 - \xi_L)/2 - \sqrt{(1+q)r_c}, \tag{1}$$

where ξ_2 and ξ_L are logarithmic derivatives of the radii of the donor and its Roche lobe with respect to its mass, $r_c \equiv R_c/a$ is the relative circularisation radius. In between these two limits, dynamical stability of mass transfer depends on the efficiency of spin–orbit coupling.

An additional complication is brought in by the fact that the surface luminosity of the WD, as determined by the mass deposition in the gravitational field of the accretor, cannot exceed the Eddington limit. In the specific case of the gravitational potential of IDD, if $\dot{M}_a$ is super-Eddington, the excess of the matter remains in the potential well of the accretor, the released energy heats it and may cause it to expand and form a common envelope in which the two components will merge (Han & Webbink 1999). Numerical experiments by Marsh et al. (2004) showed that in the case of weak tidal coupling stable mass transfer is possible if initial mass ratio is $\lesssim 0.25$ for $M_{CO} \approx 0.6\,M_\odot$ and $\lesssim 0.21$ for $M_{CO} \approx 1.0\,M_\odot$. In the limit of very strong tidal coupling, the critical values of mass ratios become ≈ 0.45 and ≈ 0.3, respectively.

The Eddington luminosity limit for $\dot{M}$ is more stringent than the dynamical stability one; therefore initial mass-transfer rates in AM CVn systems should be between 10^{-6} and $10^{-5}\,M_\odot\,\mathrm{yr}^{-1}$. However, it is possible that, even if $\dot{M}_a < \dot{M}_{Edd}$, it could exceed the maximum rate of He-burning at the base of the He-envelope (Nomoto 1982). In the latter case a red-giant-like extended envelope forms and components, most probably, merge.[1] Thus, the existing IDD should start their evolution with $\dot{M} \sim 10^{-6}\,M_\odot\,\mathrm{yr}^{-1}$ and may evolve in a Hubble time to $\dot{M} \sim 10^{-12}\,M_\odot\,\mathrm{yr}^{-1}$ as it is theoretically inferred (Tutukov & Yungelson 1979; Nelemans et al. 2001; Deloye et al. 2007) and supported by the analysis of the spectra of several AM CVn stars (Krausz et al. 2010; Gehron et al. 2014).

Along their path in M_{acc}–$\dot{M}$ plane, accretors of IDD may experience stable He-burning, burning via mild and strong flashes and, in principle, enter the regime of dynamical flashes (for a systematical study of the burning regimes of the accreted He, see Piersanti, Tornambé & Yungelson 2014, hereafter Paper I). We define a flash

as 'strong', if in its course the WD overflows its Roche lobe. Otherwise, the flash is defined as 'mild'. Interpolation between the models computed with constant $\dot{M}_a$ suggests that in the course of the evolution AM CVn stars experience ~ 10 strong non-dynamical flashes.

Bildsten et al. (2007) paid attention to the circumstance that, with decreasing $\dot{M}$, the mass to be accreted to get He-ignition, ΔM_{ign}, increases. Thus, there should exist the strongest 'last flash'. Further, the mass of the donor becomes smaller than ΔM_{ign}. The last flash may become dynamical and result in a detonation, if the thermonuclear time-scale, $\tau_{nuc} = c_P T/\epsilon_{nuc}$, becomes shorter than the local dynamical time, $\tau_{dyn} = H_P/c_s$, where H_P is the pressure scale-height and c_s is the sound speed. Due to the physical conditions existing in the accreting WD, the detonation produces short-living radioactive isotopes of Cr, Fe, and Ni. As well, ejected mass is small. The brightness of the event is comparable to subluminous SNe Ia, but its rise-time is only 2–10 d. Extrapolating the measured local birth-rate of AM CVn stars and assuming that all of them produce a visible event, Bildsten et al. (2007) estimated that the latter may occur once in 5000–15 000 yr in a $10^{11}\,M_\odot$ E/S0-type galaxy, i.e. at a rate of $\sim 1/10$th of the inferred SNe Ia rate in them. Having in mind the low luminosity of these faint supernovae and the quoted occurrence rate, Bildsten et al. dubbed them 'SNe .Ia' (1/10th of brightness at 1/10th of total rate). According to later calculations (Shen & Bildsten 2009), such faint thermonuclear SNe are likely to occur if masses of accretors are in the range (0.8–1.2) $M_\odot$. We note that, according to existing population synthesis results (Nelemans et al. 2001), AM CVn stars with such masses of the accretors should be extremely rare. Therefore, SNe .Ia may be substantially more rare events than estimated by Bildsten et al. At the moment, none of several suggested SNe .Ia candidates is definitely confirmed (Drout et al. 2013).

In the model of evolution of IDD above, it was assumed that *mass transfer is continuous*. Recently, the authors of the present study suggested to account in the computation for the effect of mass and momentum loss from the binaries due to the RLOF by the accretor during outbursts (Paper I). It was assumed that the matter leaving the system has specific angular momentum of accretor.[2]

In Paper I, a grid of accretor masses and constant accretion rates was explored. In the present paper we consider the response to the accretion for time-dependent $\dot{M}$, appropriate to AM CVn stars with WD donors. As we show below, the RLOF episode and the associated mass and angular momentum loss from the system lead to the interruption of mass transfer, thus resulting, after the flash, in epochs of cooling of accretor which change the character of thermal flashes and the course of evolution of the binaries under consideration. In Section 2 we present our model and justify the selection of computed evolutionary sequences; results are described in Section 3. Discussion and conclusions follow in Section 4.

2 SELECTION OF INITIAL BINARIES AND COMPUTATIONAL ASSUMPTIONS

Considerations of the mass transfer stability, of the limits imposed on to the initial $\dot{M}$ by the Eddington luminosity and of the possible formation of red-giant-like envelope suggest that the precursors

---

[1] We note that a rigorous consideration of the net angular momentum change following ballistic ejection of a particle, its motion and accretion (Sepinsky & Kalogera 2014), as well as the accounting for angular momentum exchange between the spins of the components and the orbit (Kremer, Sepinsky & Kalogera 2015) resulted in a slight change of the above-mentioned conditions for dynamical stability of mass transfer. In any case, the effects of the Eddington luminosity and the existence of a limiting He-burning rate are of higher value than these corrections.

[2] To some extent, a similar evolutionary scheme was considered for semidetached WD+He-star systems by Yoon & Langer (2004) and Brooks et al. (2015); as well, it resembles the scenario of evolution of cataclysmic variables with 'hibernation'.

of WD-family of AM CVn stars are detached double-degenerate (WD+WD) systems with rather extreme mass ratios and massive accretors. Such binaries are observed as detached binary 'extremely low-mass' white dwarfs (ELM), which harbour an He WD with mass below $\simeq 0.2$ M$_\odot$ and a much more massive (presumably) CO companion; some of them have merger time less than the Hubble time (see e.g. Brown et al. 2013; Kilic et al. 2014).

Currently, several systems are observed, which may be considered as proper candidate precursors of AM CVn stars (note, here we call 'primary' the more massive invisible component with M_1.). The first candidate is eclipsing binary SDSS J075141.18−014120.9 with P_{orb}= 1.9 h, $(M_2 + M_1)$/M$_\odot$ = $(0.19 \pm 0.02) + (0.97^{+0.06}_{-0.01})$ and expected merger time $\simeq$160 Myr (Kilic et al. 2014). Another 'best' candidate is the eclipsing detached binary NLTT 11748 with P_{orb}= 5.6 h and estimated mass of the secondary ranging from $M_2 = (0.136 \pm 0.007)$ to (0.162 ± 0.007) M$_\odot$ and, correspondingly, mass of the primary from $M_1 = (0.707 \pm 0.008)$ to (0.740 ± 0.008) M$_\odot$ (Kaplan et al. 2014). Several candidate systems are single-lined and for them only lower limits of M_1 are available. Among them are SDSS J1741+6526 − P_{orb}= 1.47 h, $M_2 = 0.17$ M$_\odot$, $M_1 \geq 1.11$ M$_\odot$ (Kilic et al. 2014); SDSS J1141+3850 − $P_{orb} \approx 6.23$ h, $M_2 = 0.17$ M$_\odot$, $M_1 \geq 0.76$ M$_\odot$; SDSS J1238+1946 − $P_{orb} \approx 5.46$ h, $M_2 = 0.17$ M$_\odot$, $M_1 \geq 0.64$ M$_\odot$; SDSS J2132+0754 − $P_{orb} \approx 6.01$ h, $M_2 = 0.17$ M$_\odot$, $M_1 \geq 0.95$ M$_\odot$ (Brown et al. 2013). Yet another candidate with less certainly estimated parameters is SDSS 1257+5428 − P_{orb}= 4.55 h, $M_2 \sim 0.2$ M$_\odot$, $M_1 \sim 1$ M$_\odot$ (Kulkarni & van Kerkwijk 2010; Marsh et al. 2011). At the end, other candidate AM CVn systems may be hidden among observed sdB stars, deemed to evolve into CO WDs with mass $\gtrsim 0.5$ M$_\odot$, with low-mass WD companions, like PG 1043+760 − P_{orb} = 2.88 h, $M_2 \geq 0.101$,M$_\odot$, SDSS J083006+47510 − P_{orb} = 3.552 h, $M_2 \geq 0.137$,M$_\odot$ (Kupfer et al. 2015).

Having in mind the parameters of candidate AM CVn systems and for the sake of comparison with computations in Paper I, in the current work we selected the following donor and accretor combinations: (M_{don}, M_{acc}) = (0.17,0.60), (0.15,0.92), (0.20,1.02) M$_\odot$. In the following, we address the sequences of models for these systems as S060+017, S092+015, and S102+020, respectively. The initial CO WD models have been obtained by evolving the '*heated Models*' M60, M092 and M102 from Paper I along the cooling sequence down to the luminosity level $L = 0.01$ L$_\odot$.

Some relevant physical quantities for these binary WDs are listed in Table 1. The donors are modelled as zero-temperature objects with Eggleton's Mass-Radius relation (see Verbunt & Rappaport 1988). In the computation we neglect possible effects of finite initial entropy of the He WDs (Deloye & Bildsten 2003; Deloye et al. 2007); they are discussed in Section 4. We do not consider the effects related to the possible presence of a thin hydrogen layer at the surface of the white dwarfs when they come into contact (D'Antona et al. 2006; Deloye et al. 2007; Kaplan, Bildsten & Steinfadt 2012; Shen, Guillochon & Foley 2013; Shen 2015) and consider accretion of He only.

3 RESULTS

At the beginning of the computation, the two components of each system are put in contact (i.e. $R_{don}^{Roche} = R_{don}$). At each time-step, the angular momentum loss via GWR is computed, so that the donor overfills its own Roche lobe. As a consequence, mass is removed in order to restore the condition $R_{don} = R_{don}^{Roche}$ and it is transferred conservatively to the accretor. If and when the accretor overfills its

Table 1. Physical properties of the initial binary systems considered in the present work. We list the separation a, the mass of the donor M_{don}, the mass of the accretor M_{acc} and some physical properties of the accretors, namely the mass extension of the He-deprived core M_{CO}, the mass extension of the more external layer where the helium abundance by mass fraction is larger than 0.05 ΔM_{He}, the temperature T_c in K and the density ρ_c in g cm^{-3} at the centre, the surface luminosity L, the effective temperature T_{eff} in K and the surface radius R. In the last row we report the cooling time t_{cool} defined as the time elapsed from the bluest point along the loop in the HR diagram and the epoch of the initial model considered in the current work.

Label	S060+017	S092+015	S102+020
a (in 10^{-2}R$_\odot$)	7.599	9.222	7.965
M_{don} (in M$_\odot$)	0.170	0.150	0.200
M_{acc} (in M$_\odot$)	0.596 78	0.919 62	1.020 467
M_{CO} (in M$_\odot$)	0.5158	0.9114	1.0158
ΔM_{He} (in 10^{-2}M$_\odot$)	1.551	0.389	0.056
$\log (T_c)$	7.2820	7.1478	7.2329
$\log (\rho_c)$	6.5626	7.3378	7.6109
$\log (L/L_\odot)$	− 2.0077	− 2.1163	− 2.0322
$\log (T_{eff})$	4.2102	4.2640	4.3148
$\log (R/R_\odot)$	− 1.9012	− 2.0633	− 2.1228
t_{cool}(in 10^8 yr)	1.647	2.767	2.889

own Roche lobe, due to evolutionary reasons (e.g. the onset of an He-flash), mass is removed from the accretor, assuming that it is ejected from the system. The specific angular momentum of the lost matter is assumed to be equal to the orbital one of the accretor. The thermal response of the accretor to mass deposition is computed in detail by using an updated version of the FRANEC code, the original one being described in Chieffi & Straniero (1989). The setup of the code as well as the input physics are the same as in Paper I. The chemical composition of the matter transferred from the donor to the accretor is fixed as in Paper I by assuming that all CNO elements have been converted into ^{14}N, namely: $Y^i_{^{12}C} + Y^i_{^{13}C} + Y^i_{^{14}N} + Y^i_{^{15}N} + Y^i_{^{16}O} + Y^i_{^{17}O} + Y^i_{^{18}O} = Y^f_{^{14}N}$, where Y_j is the abundance by number of the *j*-isotope and the superscripts *i* and *f* refer to the initial MS star and the final He-donor WD, respectively. In Fig. 1 we show the profiles in the $\rho - T$ plane for the accretors in our models at the beginning of the mass-transfer process while in Fig. 2 we plot as a function of the WD mass fraction the mass fraction abundances of ^{4}He, ^{12}C and ^{16}O in the most external layers of the accretors for the same structures.

When the mass transfer starts, the evolution of the accretors in the three considered systems is quite similar, as illustrated in Fig. 3, where we show the evolutionary tracks in the HR diagram for the CO WDs in the investigated systems. Along the tracks, we mark with different symbols several important epochs. For each point we list in Table 2 some relevant physical properties of the accretors and of the binaries.

When the matter falls on to the accretor, it delivers gravitational energy that is locally stored as thermal energy and triggers the evolution backward along the cooling sequence. The heating determined by mass deposition drives to He-ignition.[3] The maximum luminosity attained during this phase depends mainly on the relative efficiency of the heating by accretion and the inward thermal diffusion; the former is determined by the accretion rate, while the latter depends on the thermal structure of the He-buffer. As the He-burning

---

[3] Consistently with Paper I, we individuate the ignition epoch as the one when the nuclear energy per unit of time delivered by He-burning is 100 times the surface luminosity.
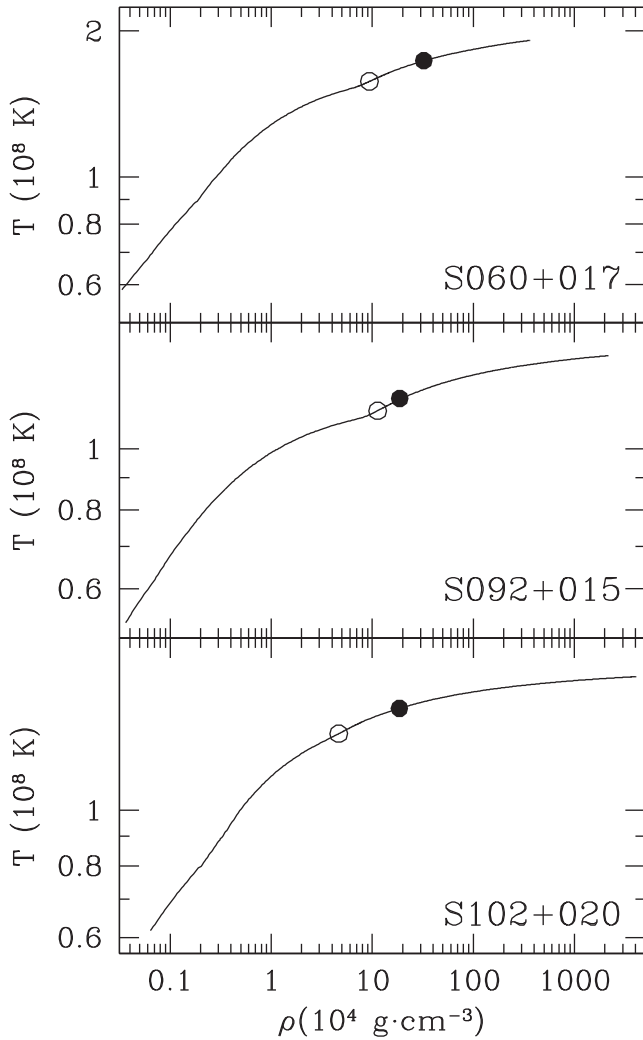
Figure 1. Profiles in the $\rho - T$ plane for the accreting CO WDs at the beginning of the mass-transfer process. Each panel refers to a different initial binary system, as labelled. Filled circles mark the He/CO interface while open ones the point where $X(\mathrm{He}) = 0.05$, roughly corresponding to the He-burning shell.
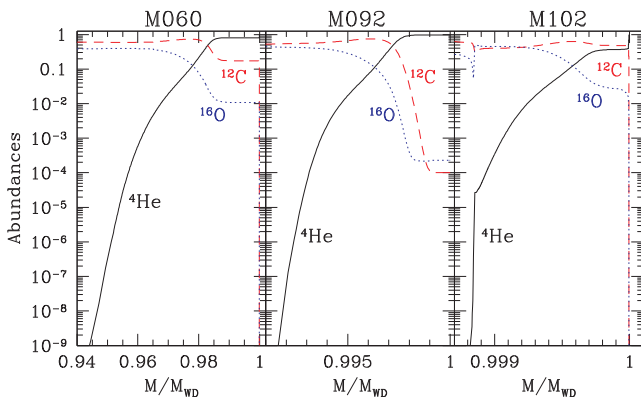

Figure 2. Mass fraction abundances of ^{4}He (solid lines), ^{12}C (dashed lines), and ^{16}O (dotted lines) in the most external layers of the accretors in the three considered binary systems. Abscissa represents the mass fraction.
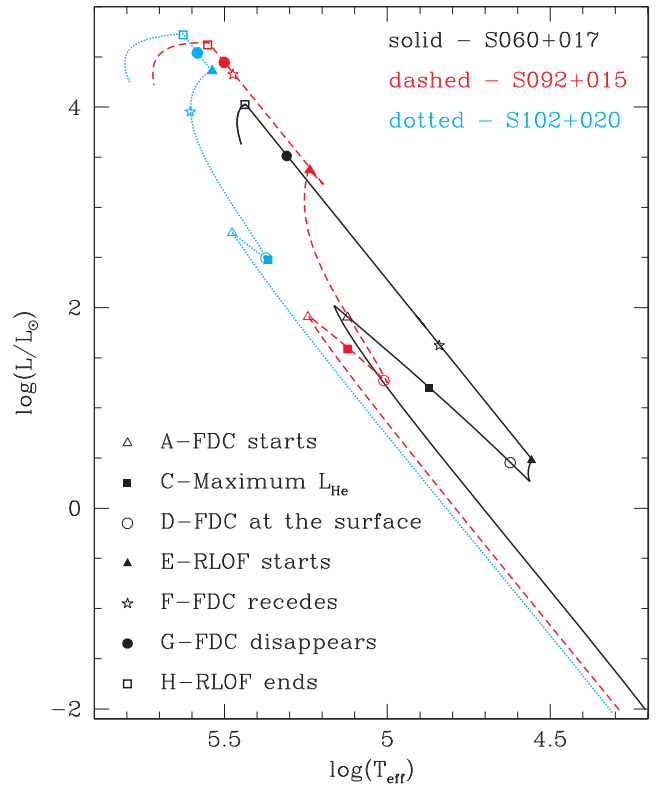
Figure 3. Evolution in the HR diagram of the accretors in the three binary systems listed in Table 1. Along the tracks some points corresponding to certain epochs in evolution are marked by different symbols and letters (see Table 2). 'FDC' means flash-driven convection.

shell has partially degenerate physical conditions, a thermonuclear runaway occurs, driving to a very powerful non-dynamical He-flash. As discussed in Paper I, this first flash represents a sort of 'heating' mechanism which alters the thermal content of the whole He-buffer above the CO core and sets in the physical conditions suitable for quiescent He-burning. The latter could occur only after the flashing structures have attained their locations in the HR diagram corresponding to a post AGB-star with the same CO core and He-buffer masses. So this first He-flash represents the analogue in real binary systems of the 'heating procedure' adopted in Paper I.

The energy delivered by the He-flash cannot be removed via radiative transfer and, hence, a convective shell forms very soon (point A in the HR diagram) and rapidly attains the stellar surface (point D). Hence, the huge amount of nuclear energy delivered by the He-flash is injected into the whole He-rich buffer above the He-burning shell, whose thermal content becomes too large for a compact configuration as that of the flashing objects. In order to dissipate the too large thermal energy stored in the He-rich mantle the accretors start to expand. If the flashing structure would be isolated in the space, it could evolve freely, increasing its luminosity and, then, should expand to very large dimensions, thus dissipating a part of its thermal energy via mechanical work and finally reaching at the He-shell, the physical conditions suitable for quiescent He-burning. But the objects considered in the present work are embedded in compact binary systems, so that they overfill their own Roche lobe very soon (point E). The following evolution of the accretors occurs inside 'the Roche lobe finite space', so that all the matter passing through the critical Roche surface is lost by the stars and, hence, by the binary systems. At the onset of the RLOF

Table 2. Physical properties of the accretors in the binary systems listed in Table 1 at same selected epochs during the first He-flash episode. The various times are: A – onset of the flash-driven convective shell; B – ignition of He-burning; C – maximum luminosity of the He-burning shell; D – flash-driven convective zone attains the stellar surface; E – beginning of the RLOF episode; F – flash-driven convective shell recedes from the stellar surface; G – flash-driven convective shell disappears; H – end of the RLOF episode; I – resumption of the mass transfer from the donor. For each epoch of each binary system we list surface luminosity $L/L_\odot$ and temperature T_{eff}, the mass coordinate of the He-burning shell M_{He} in $M_\odot$, the temperature T_{He} in 10^8 K, the density ρ_{He} in $10^4 g \cdot cm^{-3}$ and luminosity L_{He} in erg s^{-1} of the He-burning shell, the separation of the system a in $10^{-2} R_\odot$, the total mass of the accretor M_{acc} in $M_\odot$, and of the donor M_{don} in $M_\odot$, the time elapsed between two successive epochs Δt in yr. For each considered binary system we report also the amount of mass transferred from the donor to the accretor ΔM_{tran} in 10^{-3} $M_\odot$, the mass lost during the RLOF ΔM_{lost} in 10^{-3} $M_\odot$ and the corresponding value of the retention efficiency η_{acc}. Note, negative Δt for events D and F in S102+020 sequence mean that they happen *before* event E. The last block of data refers to the 'Cold' S060+017 model described in Section 3.4.

	A	B	C	D	E	F	G	H	I
				S060+017					
$\log(T_{eff})$	5.128	5.127	4.873	4.625	4.560	4.843	5.311	5.439	4.864
$\log(L/L_\odot)$	1.896	1.893	1.199	0.454	0.478	1.622	3.513	4.024	0.715
$M_{He}/M_\odot$	0.601 76	0.600 74	0.599 45	0.599 44	0.599 42	0.599 20	0.598 01	0.597 48	0.589 97
ρ_{He}	7.878	7.896	2.128	1.250	0.770	0.174	0.172	0.255	5.249
T_{He}	1.235	1.343	3.260	3.539	3.579	2.893	2.183	1.638	0.605
$\log(L_{He}/L_\odot)$	2.984	3.894	10.278	9.745	9.210	6.406	4.794	2.738	−6.119
a (in $10^{-2} R_\odot$)	8.592	8.592	8.593	8.593	8.593	8.734	8.8230	8.886	8.504
$M_{acc}/M_\odot$	0.625 59	0.625 60	0.625 61	0.625 61	0.625 60	0.613 16	0.605 57	0.600 18	0.600 18
$M_{don}/M_\odot$	0.141 19	0.141 18	0.141 17	0.141 17	0.141 17	0.141 17	0.141 17	0.141 17	0.141 17
Δt (yr)	55 637.0	42.4986	12.9458	0.0006	0.0018	0.3910	15.2389	54.1418	23 945.8

$$\Delta M_{tran} = 28.824 \qquad \Delta M_{lost} = 25.427 \qquad \eta_{acc} = 0.118$$

	A	B	C	D	E	F	G	H	I
				S092+015					
$\log(T_{eff})$	5.246	5.245	5.124	5.013	5.245	5.481	5.509	5.554	5.097
$\log(L/L_\odot)$	1.909	1.908	1.588	1.272	3.376	4.324	4.439	4.620	1.286
$M_{He}/M_\odot$	0.922 81	0.922 49	0.922 05	0.922 04	0.921 98	0.921 56	0.916 34	0.916 00	0.916 00
ρ_{He}	11.594	11.659	4.156	3.702	0.724	0.164	0.171	0.300	7.417
T_{He}	1.248	1.354	4.073	3.765	3.949	2.930	29098	2.812	1.062
$\log(L_{He}/L_\odot)$	3.052	3.910	11.311	11.177	8.767	5.462	5.319	3.910	−4.224
A (in $10^{-2} R_\odot$)	9.651	9.651	9.651	9.651	9.651	9.713	9.718	9.767	9.615
$M_{acc}/M_\odot$	0.929 85	0.929 85	0.929 85	0.929 85	0.929 85	0.923 07	0.922 53	0.917 07	0.917 07
$M_{don}/M_\odot$	0.139 77	0.139 77	0.139 77	0.139 77	0.139 77	0.139 77	0.139 77	0.139 77	0.139 77
Δt (yr)	24 468.8	11.4436	3.374 08	0.000 06	0.003 25	0.836 78	3.345 15	45.7288	6028.94

$$\Delta M_{tran} = 10.230 \qquad \Delta M_{lost} = 12.787 \qquad \eta_{acc} = -0.250$$

	A	B	C	D	E	F	G	H	I
				S102+020					
$\log(T_{eff})$	5.479	5.479	5.368	5.375	5.540	5.607	5.585	5.629	5.495
$\log(L/L_\odot)$	2.744	2.743	2.477	2.493	4.361	3.954	4.541	4.721	2.808
$M_{He}/M_\odot$	1.020 90	1.020 78	1.020 68	1.020 70	1.020 51	1.020 70	1.020 10	1.020 36	1.019 83
ρ_{He}	4.560	4.535	1.395	1.445	0.455	0.716	0.468	0.133	2.754
T_{He}	1.488	1.637	4.130	4.081	3.543	3.976	3.249	2.599	1.612
$\log(L_{He}/L_\odot)$	3.867	4.744	9.573	9.566	7.175	8.588	5.178	4.396	−0.088
A (in $10^{-2} R_\odot$)	8.020	8.020	8.020	8.020	8.020	8.020	8.029	8.030	8.016
$M_{acc}/M_\odot$	1.022 50	1.022 50	1.022 50	1.022 50	1.022 50	1.022 50	1.021 00	1.020 67	1.020 67
$M_{don}/M_\odot$	0.197 97	0.197 97	0.197 97	0.197 97	0.197 97	0.197 97	0.197 97	0.197 97	0.197 97
Δt (yr)	939.911	0.810 22	0.268 48	−0.000 01	0.050 24	−0.047 71	2.902 04	13.4218	181.015

$$\Delta M_{tran} = 2.034 \qquad \Delta M_{lost} = 1.829 \qquad \eta_{acc} = 0.101$$

	A	B	C	D	E	F	G	H	I
				S060+017 *Cold*					
$\log(T_{eff})$	5.128	5.127	4.876	4.626	4.573	4.388	4.972	5.440	4.850
$\log(L/L_\odot)$	1.883	1.880	1.195	0.450	0.534	0.660	3.399	4.027	0.642
$M_{He}/M_\odot$	0.603 18	0.602 30	0.600 89	0.600 88	0.600 87	0.600 61	0.597 48	0.595 40	0.590 50
ρ_{He}	7.907	7.883	2.154	1.258	0.757	0.186	0.169	0.266	4.113
T_{He}	1.233	1.341	3.271	3.558	3.596	3.022	2.304	1.664	0.568
$\log(L_{He}/L_\odot)$	2.964	3.882	10.317	9.770	9.204	6.714	5.605	2.716	−7.129
A (in $10^{-2} R_\odot$)	8.626	8.627	8.627	8.627	8.627	8.667	8.812	8.958	8.520
$M_{acc}/M_\odot$	0.626 46	0.626 47	0.626 47	0.626 47	0.626 47	0.622 97	0.610 32	0.598 03	0.598 03
$M_{don}/M_\odot$	0.140 32	0.140 31	0.140 31	0.140 31	0.140 31	0.140 31	0.140 31	0.140 31	0.140 31
Δt (yr)	58 331.2	45.0383	11.9684	0.0005	0.0019	0.2854	30.3768	66.2967	86 893.4

$$\Delta M_{tran} = 29.694 \qquad \Delta M_{lost} = 28.444 \qquad \eta_{acc} = 0.042$$

episode, due to the loss of matter and angular momentum from the systems, the orbital separation increases, therefore, the donors detach from their Roche lobes and, hence, the mass transfer halts. During the RLOF episode the accretors evolve at almost constant radii, increasing their surface luminosity and effective temperature up to when they recede definitively from their Roche lobe (point H). Since the components of the binary are now detached, mass transfer from donors to accretors can resume only after angular momentum loss by GWR shrinks the orbits, thus forcing the donors to overfill once again their Roche lobe. During the time between the end of the RLOF and the re-onset of mass accretion, accretors evolve first up to the bluest point along the loop in the HR diagram and, then, down along the cooling sequence.

For each considered system, in Table 2 we report the total mass transferred from the donor to the accretor during the first mass-transfer episode (ΔM_{tran}), the mass lost during the RLOF phase (ΔM_{lost}) and the corresponding accumulation efficiency η_{acc}, defined as in equation (5) in Paper I:

$$\eta_{\text{acc}} = 1 - \frac{\Delta M_{\text{lost}}}{\Delta M_{\text{tr1}} + \Delta M_{\text{tr2}}}, \qquad (2)$$

where ΔM_{tr1} is the amount of mass transferred up to the onset of the RLOF episode and ΔM_{tr2} the one accreted after the end of the RLOF up to the bluest point along the loop in the HR diagram.

3.1 S060+017 System

In Fig. 4 we plot for the S060+017 and S092+015 systems (the latter to be discussed in the next subsection) the dependence of the mass-transfer rate from the donor (upper panel) and the dependence of the slope of the curves $n = \mathrm{d}\log \dot{M}/\mathrm{d}\log P_{\text{orb}}$ (lower panel) on the orbital period P_{orb}. For the sake of comparison, in the lower panel we show also the n curve for a system with initial parameters equal to the ones of S060+017, but evolving completely conservatively. The figure clearly shows that thermonuclear outbursts, interrupting the mass transfer (see the previous section), virtually do not influence the common behaviour of the $\dot{M}$–P_{orb} relation for ultracompact binaries evolving under the influence of angular momentum loss by GWR. Recently, Cannizzo & Nelemans (2015), using the limit cycle accretion disc instability model, attempted to constrain semi-analytically the mass-transfer rate in AM CVn stars by fitting $\dot{M}$ to the P_{orb} limits of the accretion disc-instability range of these systems, namely 20 and 44 min. The metallicity of AM CVn stars is unknown. For the range of Z from 0.0 to 0.04, Cannizzo & Nelemans found values of n from -5.38 ± 0.3 to -5.06 ± 0.3. Though the period range of interest for the present work is below 20 min, the comparison to the results of Cannizzo & Nelemans (2015), as well as to earlier evaluations of e.g. Tutukov & Yungelson (1996); Nelemans et al. (2001), validates our computations. As it concerns the estimates of accretion rates in AM CVn-stars, they are obtained by indirect methods and can hardly constrain the $\dot{M}$–P_{orb} relation. They may be considered as 'indicators' of the proper order of magnitude of the computed $\dot{M}$, at best.

In Fig. 5 we plot the mass-transfer rate (upper panel) for the S060+017 system as well as the evolution of the temperature (middle panel) and density (lower panel) of the He-shell in the accretor as a function of time. As can be seen, after the He-flash and the related RLOF episode, mass transfer is not active and the He-burning shell cools down. When mass transfer resumes, the corresponding accretion rate is about $3.23 \times 10^{-7}\ \mathrm{M}_\odot\ \mathrm{yr}^{-1}$. Due to the deposition of matter, the He-shell starts to heat up once again, but when $\dot{M}$ becomes lower than $8 \times 10^{-8}\ \mathrm{M}_\odot\ \mathrm{yr}^{-1}$, the mass deposition becomes
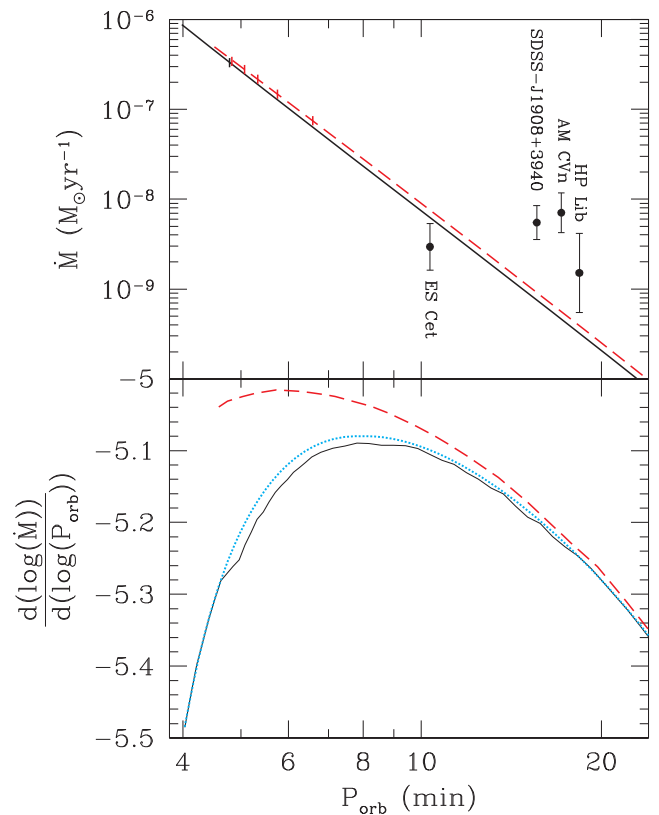

Figure 4. Upper panel: dependence on the orbital period of the mass-transfer rate from the donors in the systems S060+017 (solid line) and S092+015 (dashed line). The small vertical ticks on the curves mark the values of P_{orb} when mass transfer does not occur. In these systems the first outbursts happen at $P_{\text{orb}} = 4.792$ min and 4.830 min, respectively, and the corresponding gaps ΔP_{orb} (0.13 and 0.09 s, respectively) are too short to be noticeable in the scale of the plot. Filled circles with error bars show estimates of mass-transfer rates in observed AM CVn systems [taken from the compilation by Kotko et al. (2012)]. Lower panel: the value of $n = \mathrm{d}\log \dot{M}/\mathrm{d}\log P_{\text{orb}}$ for the S060+017 and S092+015 systems (solid and dashed lines, respectively). The dotted line shows the n profile for the case of completely conservative mass-exchange in a $(0.60+0.17)\ \mathrm{M}_\odot$ system.

unable to balance the cooling and the accretor further evolves along its cooling sequence. Thus, despite the fact that quite a substantial amount of matter may still be transferred to the CO WD in this system (about $0.14\ \mathrm{M}_\odot$), the nuclear evolution of the binary is terminated. Though, it will retain its status of AM CVn star.

At variance with the results discussed above, the 'Heated Model' M060 in Paper I, corresponding to the accretor in the S060+017 system, after the first He-flash, burns helium quiescently for $\dot{M} \geq 1.5 \times 10^{-7}\ \mathrm{M}_\odot\ \mathrm{yr}^{-1}$. However, it has been noted that the present computation differs from those in Paper I in many regards. First of all, in Paper I the accretion rate was kept strictly constant in each simulation and mass deposition was restarted soon after the end of the RLOF, thus preventing substantial cooling of the He-buffer. In addition, the adopted value for the Roche lobe radius ($10\ \mathrm{R}_\odot$) was definitively larger than the one proper to the self-consistent computation of the S060+017 system.

In order to illustrate the origin of such a difference, we computed two models, arbitrarily varying the value of the separation during the evolution of the S060+017 system. In the first one we reduced the value of the separation after the end of the RLOF episode in such
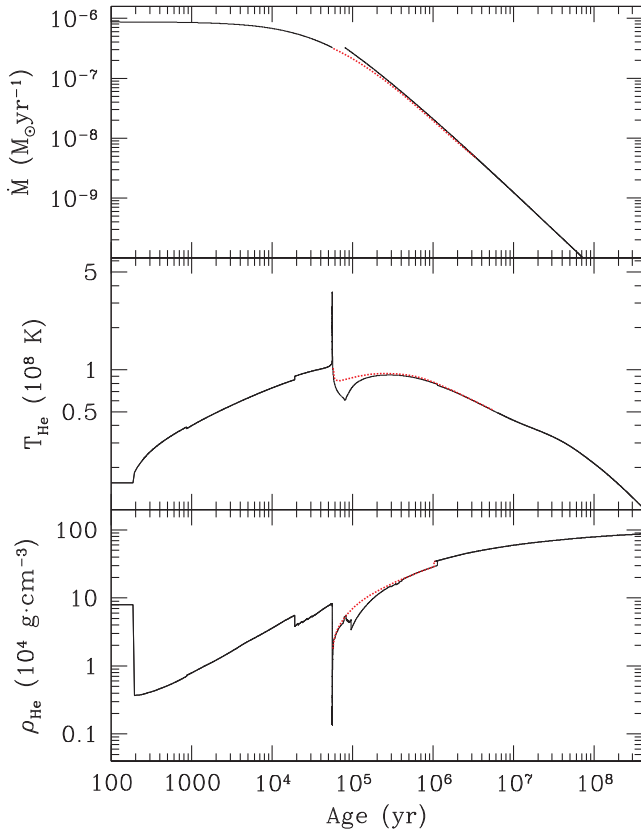
Figure 5. Time evolution of the accretion rate ($\dot{M}$ – upper panel) of the He-shell temperature (T_{He} – middle panel) and density (ρ_{He} – lower panel) of the accretor in the binary system S060+017. Dotted lines refer to the evolution of the same object, but starting to accrete mass soon after the end of the RLOF. For more details see text.

Figure 6. Upper panel: time evolution of the flash-driven convective shell (grey zone), of the total mass (dashed line) and of the mass coordinate of the He-burning shell (solid line) for the accretor in the S060+017 system. The vertical dashed line in the upper panel marks the end of the RLOF episode. Lower panel: behaviour of the same quantities at the same time in the Test model where RLOF occurs later.

a way that mass transfer resumed immediately. The time evolution of the mass-transfer rate and of the temperature and density of the He-burning shell for this model is displayed by dotted lines in Fig. 5. The prompt onset of mass accretion prevents the decrease of the temperature of the He-burning shell below $\sim 8.3 \times 10^7$ K, but, in any case, as $\dot{M}$ continuously decreases, the accretor never attains the physical conditions suitable for the re-ignition of helium. This numerical experiment clearly suggests that the origin of the difference between the present computation and the corresponding one in Paper I depends on the different thermal content of the post-RLOF structure.

To make this more clear, we performed the second run (Test model) increasing arbitrarily by a factor of 100 the binary separation at the epoch of the onset of the RLOF overflow in the S060+017 system. Note that, as a consequence of such a variation, the Roche lobe of the accretor became $\simeq 4R_\odot$, while the Roche lobe radius of the donor increased to 2.2 $R_\odot$ and, hence, the mass transfer came to a halt. In this way we constructed a model having exactly the same mass of the He-rich buffer of the accretor as in the S060+017 system, but which 'freely' expanded in the space before the onset of the RLOF, as in the computations of Paper I.

In the upper panel of Fig. 6 we show the time evolution of the flash-driven convective shell (grey area), of the total mass (dotted line) and of mass coordinate of the He-burning shell (solid line) for the accretor in S060+017 system. In the lower panel we show the behaviour of the same quantities, but for the Test model, which has larger Roche lobe. The epoch $t = 0$ corresponds to the onset of the
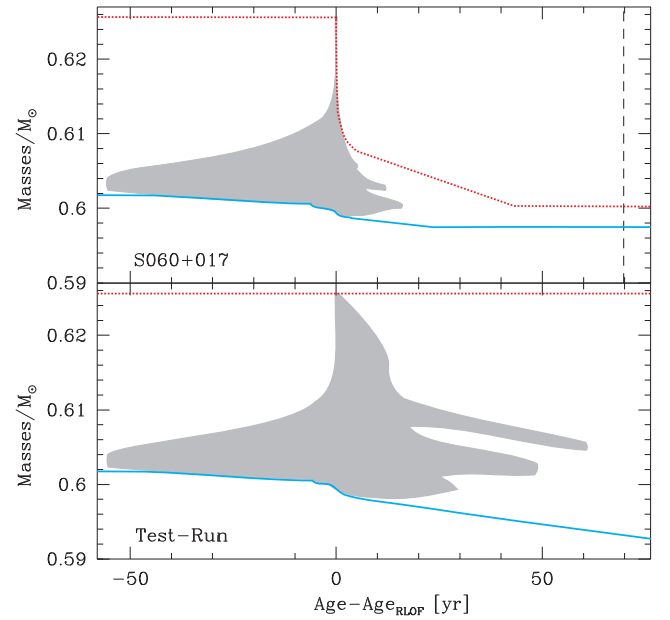
RLOF episode in the S060+017 system, while the dashed vertical line marks its end. As it is seen, the mass loss triggered by the RLOF episode determines the rapid disappearance of the convective shell. As discussed in Paper I, convection affects the evolution of the He-flash in two opposite ways: on one hand it removes energy from the inner zones of the He-rich buffer and redistributes it over the whole envelope, thus reducing the local increase of temperature and damping the thermonuclear runaway. On the other hand, convective mixing dredges down fresh helium, feeding the burning-shell and, hence, powering the flash. As a result, the strong and rapid reduction of the convective shell in the S060+017 system limits the amount of nuclear energy produced via He-burning and, hence, the resulting flash is weaker with respect to the Test model. To make this conclusion more quantitative, we define for the model S060+017 two time intervals: $\Delta t_1 = 55.468$ yr, lasting from the onset of the flash-driven convective shell to the onset of the RLOF, and $\Delta t_2 = 69.774$ yr, lasting from the onset to the end of the RLOF. In the S060+017 model during Δt_1 He-burning delivers an amount of energy equal to $\varepsilon_1 \simeq 2.678 \times 10^{48}$ erg, while during Δt_2 it delivers $\varepsilon_2 \simeq 1.639 \times 10^{48}$ erg. In the Test model, the energy delivered during Δt_2 is by a factor 2 larger ($\varepsilon_2^{TM} \simeq 3.219 \times 10^{48}$ erg).[4]

Fig. 6 also demonstrates that the extension and lifetime of the flash-driven convective shell affects the heating of the layers below the He-burning shell. This is clearly indicated by the inward shift of the He-burning shell (see solid lines in Fig. 6): a larger amount of thermal energy produced via He-burning determines a more efficient heating of the underlying zones and, hence, a deeper inward shift of the He-burning shell itself.

---

[4] Note that during Δt_2, the surface radius of the accretor in the S060+017 system remains practically unaltered, as it is fixed by the Roche lobe radius, while in the Test model it increases by a factor 25.
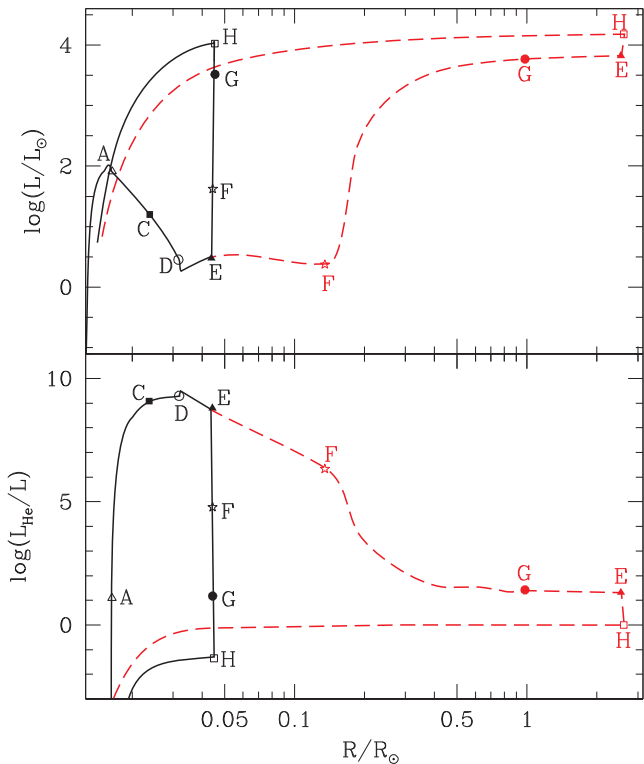
Figure 7. Dependence of the total luminosity L (upper panel) and ratio of luminosity of the He-burning shell L_{He} and total luminosity L (lower panel) on the radius of the CO WD in the sequence S062+017 during the He-flash. S062+017 system is shown with solid lines, and the Test model with dashed ones. In the evolutionary phase where the two accretors evolve identically, dashed lines are hidden behind the solid ones. Different points and letters mark various important epochs, as in Fig. 2.

To illustrate further the difference between these two cases, i.e. between the evolution of very compact systems and that of wider ones, we present in Fig. 7 the dependence of the total luminosity of the accretor L (upper panel) and the ratio of the He-burning shell luminosity and the total luminosity L_{He}/L (lower panel) on the WD radius. The evolutionary paths of two accretors coincide up to RLOF epoch in the S060+017 system. In the latter, soon after the onset of the RLOF, convection is aborted and the He-rich layers above the He-burning shell, previously heated by the flash, are lost in a short time-scale (Fig. 6). This almost extinguishes He-burning very rapidly and the only energy source to maintain thermal equilibrium becomes contraction. This can be seen in the lower panel of Fig. 7, showing that after the RLOF episode in the system S060+017 the ratio L_{He}/L becomes $\simeq 1/20$. As He-burning dies completely, contraction will remain the only energy source balancing the radiative losses from the surface since He is never reignited because of the cooling of the He buffer due to the interruption of mass transfer and, later on, to the insufficient heating via accretion (Fig. 5). In the Test model, convection continues to support the He-burning shell and, consequently, the delivered energy drives the expansion of the WD He-rich envelope to the large Roche radius. The dwarf recedes from its Roche lobe when the energy produced via He-burning equates the energy losses from the surface. However, this occurs slower than in the case of the tight system – for the same luminosity level after the RLOF, the accretor in the S062+017 model is more compact than in the Test model (upper

panel of Fig. 7). Later on, the two models converge to the same evolutionary path.

The difference illustrated above has a sizable effect on the retention efficiency of the two models. In particular, in the Test model a larger amount of nuclear energy is delivered before the onset of the RLOF episode, so that the whole He-buffer above the CO core is heated more than in the S060+017 system. As a consequence, the He-burning shell can move inwards; moreover, even if a part of the energy injected in the He-rich buffer is dissipated via mechanical work (expansion to larger radius), the thermal content of the He-rich mantle remains very large. As a matter of fact, a larger amount of matter is lost during the RLOF episode in the Test model ($\Delta M_{lost} = 2.7 \times 10^{-3}$ M$_\odot$), so that the corresponding retention efficiency reduces to $\eta_{acc} = 0.065$ (about 45 per cent lower than the one obtained for the S060+017 system). In Paper I we found that the 'heating' flash in the M060 *Cool model* erodes also part of the pre-existing He-rich buffer, while in the Test model we find a small, but in any case positive, retention efficiency. Such a difference reflects the different values of $\dot{M}$ adopted for the above-mentioned models: in Paper I we use $\dot{M} = 10^{-7}$ M$_\odot$ yr^{-1}, while in the Test model the accretion rate is definitively larger: initially it is as high as 8.8×10^{-7} M$_\odot$ yr^{-1} and, in any case, it remains larger than 3.3×10^{-7} M$_\odot$ yr^{-1}. In Paper I we explored the dependence of η_{acc} on the assumed Roche lobe radius by varying the latter in the range 1–45 R$_\odot$ and we found that the difference in the estimate of retention efficiency is smaller than 7–8 per cent. Such a conclusion is appropriate for binaries with relatively massive He-star donors, but, as demonstrated above, not for low-mass compact stars.

To summarize, in the S060+017 system, due to the small separation, the first He-flash does not result in an efficient heating of the layers above the CO core, so that the following evolution proceeds substantially differently from what is derived in Paper I.

3.2 S092+015 system

The first flash in the S092+015 system is much stronger than in the other systems, as clearly displayed in Fig. 8, where we plot as a function of the evolutionary time three quantities characterizing the He-flash for all the systems listed in Table 2: the He-burning luminosity L_{He} (upper panel), the total energy released during the flash E_{He} (middle panel), and the 'specific energy' of the flash e_{He} (lower panel), defined as the ratio of E_{He} and mass of the He-rich zone.

The maximum luminosity in the burning shell L_{He} attained during the flash is 10 times larger than for the S060+017 system and about 50 times larger than for the S102+020 one (see also Table 2). Such an occurrence is not related to the physical properties of the He-shell and to the thermal content of the underlying CO core at the onset of the mass transfer, but is determined by the adopted combination (M_{don}, M_{acc}) which sets the value of $\dot{M}$ after contact. At the beginning of the mass transfer, $\dot{M}$ for the S092+015 system is $\simeq 5.0 \times 10^{-7}$ M$_\odot$ yr^{-1} while for the S060+017 and S102+020 systems it is 8.8×10^{-7} M$_\odot$ yr^{-1} and 2.2×10^{-6} M$_\odot$ yr^{-1}, respectively. As a consequence, the compressional heating of the He-buffer occurs at a lower rate so that at the onset of the He-flash the He-shell has more degenerate physical conditions (see the values of ρ_{He} and T_{He} listed in column B of Table 2).

After the first He-flash, at the re-onset of mass transfer $\dot{M} \simeq 3.5 \times 10^{-7}$ M$_\odot$ yr^{-1}; according to Paper I, the same initial mass WD, model M092, after the 'heating flash' experiences strong He-flashes for $\dot{M} \leq 5 \times 10^{-7}$ M$_\odot$ yr^{-1}. The S092+015 system
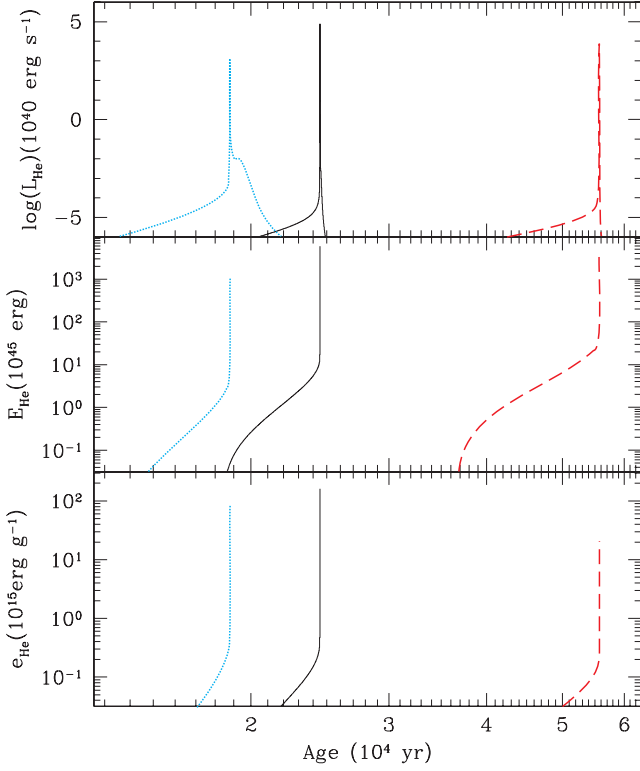
Figure 8. Comparison of the properties of the first flash in the S060+017 (dashed lines), S092+015 (solid lines), and S102+020 (dotted lines) systems. The panels (top to bottom) show the luminosity of the He-burning shell of accreting dwarf, the total energy released during the flash, and the 'specific energy' of the flash (see the text for details). The age of the S102+020 system has been arbitrarily increased by 1.9×10^4 yr.

undergoes other four strong non-dynamical He-flashes before a massive degenerate object is formed (see Table 3 and Figs 9 and 10). In Table 3 we list selected physical quantities of the accretor during the five He-flashes experienced by this system.

By adopting for $\dot{M}$ the mean value before the second flash reported in Table 3 and interpolating the data reported in table 4 of Paper I we obtain $\eta_{\rm acc} \sim 0.61$, definitively larger than the value we derive in the present work.[5] As discussed in the case of the S060+017 system, such a discrepancy has to be ascribed to the non-efficient heating of the He-layer during the first He-flash due to the sudden and sharp decrease of the mass extension of the flash-driven convective shell. When mass transfer resumes after the fifth flash, $\dot{M} = 7.25 \times 10^{-8}$ M$_\odot$ yr^{-1} and the He-shell starts to heat up once again. At $\dot{M} \sim 4 \times 10^{-8}$ M$_\odot$ yr^{-1} the accretor enters the regime which for the actual $M_{\rm WD}$ and constant $\dot{M}$ would correspond to dynamical flashes (Paper I). In the case under analysis, as $\dot{M}$ continuously decreases, neutrino cooling starts to dominate over the compressional heating and no additional He-flashes (dynamical or not) are ignited. Hence, accretor turns into a nuclearly inert degenerate object which gradually increases its mass.

---

[5] According to the discussion in section 3.1 of Paper I, the evolutionary outcome of WDs accreting mass with a time-dependent accretion rate depends mainly on the current value of $\dot{M}$ and to a less extent on the previous thermal history. At the onset of the second He-flash in the S092+015 system we find $\dot{M} \approx 2.5 \times 10^{-7}$ M$_\odot$ yr^{-1}; for this $\dot{M}$, according to the data in table 4 of Paper I, we obtain $\eta_{\rm acc} \simeq 0.49$.

Table 3. Selected physical properties for each of the five strong pulses experienced by the accretor in the S092+015 system. $M_{\rm He}$ (the mass coordinate of the He-burning shell, M$_\odot$), $\Delta M_{\rm He}$ (the mass above the He-burning shell, 10^{-3} M$_\odot$), $P_{\rm orb}$ (the orbital period, in min), $\rho_{\rm He}$ *and* $T_{\rm He}$ (density in 10^4 g cm^{-3} and temperature in 10^8 K at the He-burning shell) refer to the epoch of He-ignition. $L_{\rm He}^{\rm max}$ is the maximum luminosity of the He-burning attained during the He-flash. $\langle \dot{M} \rangle$ is the mean value of the mass accretion rate (in 10^{-7} M$_\odot$ yr^{-1}) during the time lasting from the onset of mass transfer and the onset of the RLOF episode. $\Delta M_{\rm tran}$ and $\Delta M_{\rm lost}$ (in 10^{-3} M$_\odot$) are the amounts of mass transferred from the donor and lost by the accretor during the RLOF, respectively. $\eta_{\rm acc}$ represents the accumulation efficiency, while Δt (in yr) is the time lasting from the end of the RLOF to the re-onset of mass transfer.

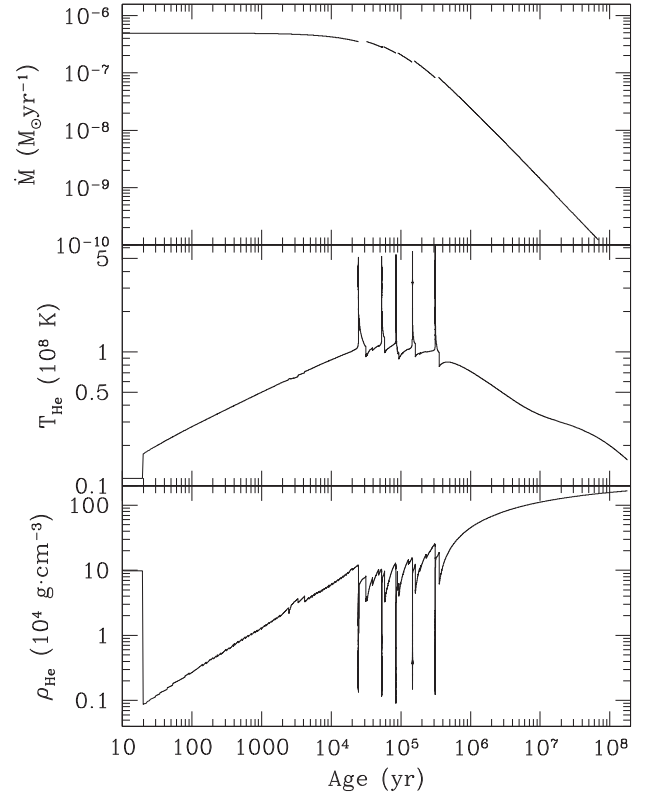|	1st	2nd	3rd	4th	5th
$M_{\rm He}$	0.9225	0.9180	0.9178	0.9189	0.9203
$\Delta M_{\rm He}$	7.362	5.887	6.851	8.935	14.170
$P_{\rm orb}$	4.830	5.069	5.331	5.753	6.588
$\rho_{\rm He}$	11.66	9.22	10.78	14.00	22.13
$T_{\rm He}$	1.354	1.385	1.367	1.289	1.205
$\log(L_{\rm He}^{\rm max}/{\rm L}_\odot)$	11.311	10.787	10.967	11.592	12.520
$\langle \dot{M} \rangle$	4.178	3.087	2.413	1.748	1.015
$\Delta M_{\rm tran}$	10.230	6.865	6.838	9.799	15.802
$\Delta M_{\rm lost}$	12.787	6.107	6.584	9.191	15.085
$\eta_{\rm acc}$	-0.250	0.110	0.037	0.062	0.045
Δt	6028.9	3434.5	4805.2	8401.0	23316.8

Figure 9. The same as in Fig. 5 but for the S092+015 system.

3.3 S102+020 system

The evolution of the S102+020 system after the first flash is quite different. Fig. 3 and Table 2 reveal that for this system the evolution during the first He-flash episode is more similar to that of a 'freely' expanding model. In fact the flash-driven convective shell attains the
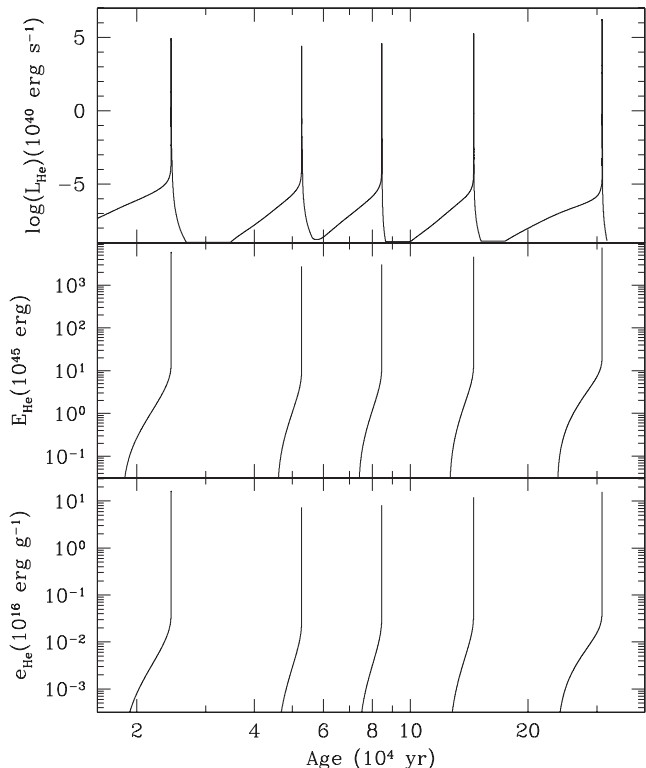
Figure 10. Comparison of the properties of subsequent flashes in the sequence S092+015. The same variables as in Fig. 8 are plotted.

Figure 11. Evolution of the S102+020 system. We report as a function of the mass transferred from the donor the mass-transfer rate $\dot{M}$ (upper panel), the luminosity of the He-burning shell (middle panel) and the mass of the accretor M_{acc} (lower panel). Vertical dashed line in the upper panel marks the transition from one accretion regime to another (see text for details).

stellar surface *before* the epoch of the maximum He-shell burning luminosity and, in addition and more importantly, the RLOF episode starts *after* the flash-driven convective zone has receded from the stellar surface (see the sequence of the various phases in Fig. 3 and the negative value of Δt for epochs D and F in Table 2). This means that the He-flash succeeds in heating the whole He-buffer to a higher level with respect to what occurs in the S060+017 and S092+015 systems. Such an occurrence is a direct consequence of the fact that, when the components in this binary system come to contact for the first time, the mass-transfer rate is very high ($\dot{M} \simeq 2.2 \times 10^{-6}$ M$_\odot$ yr^{-1}), so that gravitational energy released by accretion efficiently heats up the entire He-buffer. This determines less degenerate physical conditions at the onset of the He-flash, as compared to the other two considered systems (see ρ_{He} and T_{He} for the epochs A and B in Table 2), so that the resulting He-flash is less strong (see the value of L_{He} at the epoch C in Table 2 and Fig. 8).

When mass transfer from the donor resumes, $\dot{M}$ is still as high as $\sim 2.1 \times 10^{-6}$ M$_\odot$ yr^{-1} (see the upper panel in Fig. 11). In Paper I we found that the 'heated' M102 model accreting at such a rate experiences quiescent burning of He. On the contrary, in the present work the accretor in the S102+020 system experiences other three flashes. The flashes become progressively less strong (see the middle panel of Fig. 11) and the corresponding retention efficiency increases (see lower panel of Fig. 11). In particular, we find $\eta_{acc}=$ 0.562 for the second flash and $\eta_{acc}= 1.0$ for the third one. We classify the latter as a 'mild flash' (MF), i.e. a flash which releases so little nuclear energy that the accretor remains confined well inside its Roche lobe and no mass-loss occurs. Such a behaviour is determined by the fact that, pulse by pulse, the He-rich buffer and the most external layers of the underlying CO core heat up, thus attaining the physical conditions suitable for quiescent He-burning. The resulting evolution is completely different from that of the ac-
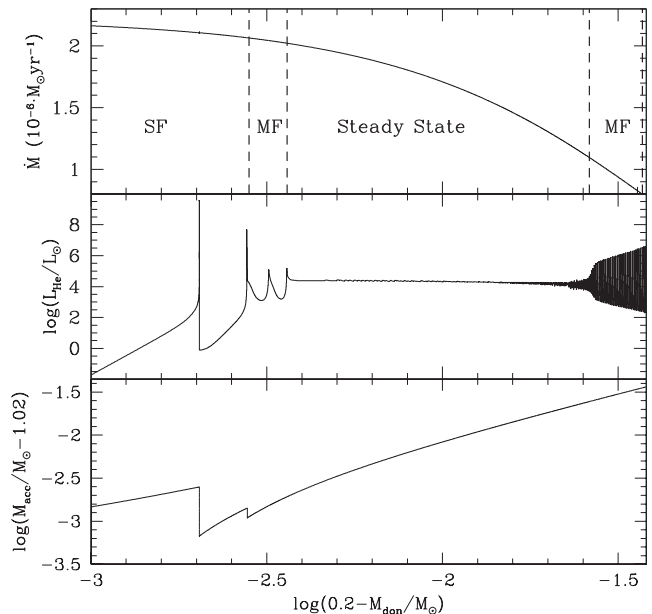
cretor in the S092+015 system and it is a direct consequence of the mass-transfer rate after the first flash episode which depends on the parameters of the initial binaries. In particular, as already mentioned before, $\dot{M}$ in the S092+015 system after the first flash should determine recurrent strong flashes also in a fully heated model with the same total mass and mass of the He-buffer (e.g. the 'heated' M092 model in Paper I). At variance, in the S102+020 system the mass-transfer rate is so high that the released gravitational energy prevents the cooling down of the He-burning shell during each inter-flash period. As displayed in Fig. 11, after four flashes the accretor reaches steady burning regime (Steady State), which lasts as long as, due to continuous decrease of the mass-transfer rate from the donor, the extension of the He-buffer above the He-burning shell reduces below a critical value and the accretor enters again the mild flashes regime. The transition from one regime to another occurs smoothly so that we arbitrarily define the value of $\dot{M}$ at which such a transition occurs as the epoch when the maximum luminosity of the He-burning shell during the He-flash becomes twice the value of the surface luminosity along the high-luminosity branch. Under this assumption we find $\dot{M}$(SS-MF)$\simeq 1.09 \times 10^{-6}$ M$_\odot$ yr^{-1}. Due to the evolution of binary parameters, the mass-transfer rate continuously decreases and when it becomes lower than $\sim 8.3 \times 10^{-7}$ M$_\odot$ yr^{-1}, after 29 MFs, Strong Flashes start again. In the upper panel of Fig. 11, the transitions from one regime to another are marked by dashed vertical lines.

The following evolution is described in Fig. 12 where we show, as a function of the accretor total mass at the bluest point along the loop, the value of the retention efficiency, and the physical conditions (temperature and density) at the epoch of the He-flashes ignition. As well, the maximum luminosity in the He-burning shell L_{He} is shown. As expected for a monotonically decreasing mass-transfer rate, η_{acc}, on average, decreases continuously (upper panel), as the physical conditions at the He-shell become more degenerate and,
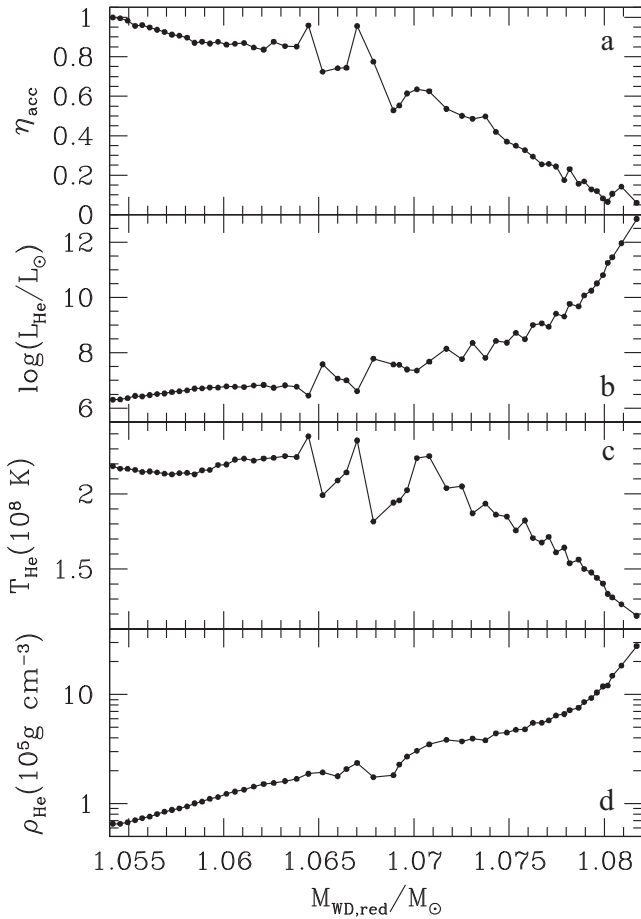
Figure 12. Evolution of the accretor in the S102+020 system during the Strong Flashes accretion regime. We report, as a function of the total mass of the accretor at the bluest point along the loop in the HR diagram ($M_{WD, blue}$), the value of the retention efficiency (panel a), the luminosity of the He-burning shell (panel b), and the temperature (panel c) and density (panel d) at the epoch of He-ignition.

hence, the strength of successive flashes increases. The general trend is defined by two main factors. On one hand, as the accretion rate decreases and η_{acc} reduces, the time-span after the end of the RLOF episode and the mass-transfer resumption increases, so that the He-buffer cools more. This determines the increase of the amount of mass to be transferred to ignite the successive He-flash which, as a result, is also stronger. On the other hand, pulse by pulse, the Roche lobe radius of the accretor increases, so that during the successive He-flashes the heating of the whole He-buffer is more efficient, as the RLOF occurs when a larger amount of nuclear energy has been delivered (see the discussion of S060+017 system and related Fig. 6). Though the evolutionary curves also exhibit irregularities whose origin depends on the complex interplay of various additional factors.

We find that after the 58th strong flash, the mass of the donor has reduced to $\sim 0.0875 M_\odot$ and that of the accretor increased to $\sim 1.0822 M_\odot$. When accretion resumes, after 181916 yr, the mass-transfer rate is $4.2 \times 10^{-8} M_\odot$ yr^{-1} and it rapidly decreases so that the compressional heating produced by accretion is not able to balance the radiative and neutrino cooling of the whole He-rich buffer. Hence, as already illustrated for the S060+017 and S092+015 systems, the accretor in the S102+020 system cools

down and the final outcome is a massive CO core surrounded by an extended He-buffer.

3.4 'Cold' S060+017 Model

In order to investigate the dependence of our results on the cooling age of the accretor, we let the '*heated model*' M060 from Paper I to cool for 2 Gyr which, according to population synthesis computations, can be considered as the typical time of formation of an AM CVn system from a pair of detached WDs (Tutukov & Yungelson 1996). After that, we start the accretion following the same procedure as above. The results are summarized in Table 2. As it can be noticed, at the beginning of the mass transfer, the physical conditions at the base of the He-burning shell are more degenerate (temperature is a factor 5 lower, while density is practically the same). Notwithstanding, the amount of mass to be transferred to ignite the He-flash is only 3 per cent larger and the ignition conditions are very similar (compare columns A and B in Table 2 for the standard and 'Cold' S060+017 Models) and the resulting He-flash has almost the same strength. During the RLOF episode the cold S060+017 system loses about 11 per cent more mass so that the final retention efficiency is lower. As a consequence, the post-RLOF episode separation is a bit larger and, hence, the time-span up to the re-onset of mass transfer increases by more than a factor of 3.5. In any case, the evolution after the He-flash episode occurs exactly as in the S060+020 system: the mass-transfer rate decreases very rapidly, so that the radiative and neutrino losses from the He-buffer become dominant and the system evolves to the formation of a massive CO WD with an extended He-rich mantle.

The results for the 'Cold' model suggest that the models we considered are representative also for systems with longer cooling age. The reason is that at the luminosity level 0.01 $L_\odot$ the physical conditions at the centre of WD and at the base of the He-rich buffer have attained an asymptotic value. Increasing the cooling age of accreting WDs from 800 Myr to (2–3) Gyr practically does not affect their reaction to accretion.[6] Such a statement is also confirmed by the computation of the evolution of the 'Cold' analogue of S092+015 system up to the onset of the first RLOF episode. The released nuclear energy was quite similar to the one in the 'hot' model, while the accreted mass was only 1.05 per cent larger. This similarity suggested us to terminate this additional extremely time-consuming computation, since we infer that the initial temperature of WD will not play any role, like in the case S060+017.

4 DISCUSSION AND CONCLUSIONS

In the present work we studied accretion from He WD donors on to CO WDs in ultracompact AM CVn binaries (IDD). At variance with our earlier study of the He-burning regimes in WDs accreting mass at constant $\dot{M}$ (Paper I), in our current analysis we adopted time-dependent accretion rates, as determined by the loss of angular momentum via GWR. As in Paper I, we assumed that if He-flashes on the accretors result in RLOF, matter is lost from the system until accretor recedes from the critical lobe. The matter leaving the system has the specific orbital angular momentum of the accretor. The systems considered in our analysis have the following properties: (i) mass-transfer rate permanently declines and (ii) accretion may be interrupted due to mass and angular momentum losses. In Paper I

---

[6] Longer formation times are not considered in the present analysis as they are not typical for AM CVn stars.

we assumed that the accretion process is almost continuous, as it resumes soon after the end of the RLOF episode. At the end, in our earlier study we preset arbitrarily the accretor Roche lobe radius, while in the present work the latter is defined by the actual parameters of the given binary system, i.e. masses of the components. The initial values of them were taken corresponding to supposed precursors of AM CVn stars – extremely low white dwarfs systems (ELM WDs). The donors were approximated as pure He-objects with zero temperature, proper to the formation time-scale of AM CVn stars ~Gyr.

The actual He-burning regime on to the accretors in IDD is defined by the interplay of several factors. The first, as in other accreting systems, is the balance between the compressional heating driven by the mass deposition and the cooling of the He-rich buffer via inward thermal diffusion and neutrino emission. The second is the permanently decreasing accretion rate. The third is the degeneracy level of the physical base of He-rich buffer. Last but not the least, the Roche lobe radius of accretors may be very small, down to several 0.01 $R_\odot$.

As expected (see the discussion in Paper I), we found that after the onset of mass transfer on to the accretors, the He-burning shell above the CO core heats up and, when the nuclear time-scale for 3α-reactions becomes shorter than the local thermal adjustment time-scale, a nuclear flash occurs. Due to the degenerate physical conditions, this first flash is strong and it drives to a significant expansion of the star. It is worth noticing that this first flash is the equivalent in the real world of the artificial initial *heating* flash used in the studies of He-burning on to WDs in order to mimic post-AGB objects. However, in a typical AM CVn system the accretor *should* be cold, since the time-scale of AM CVn stars formation is of the order of 1 Gyr. As a matter of fact, such a flash results in a RLOF by the accretor and drives to the loss of mass and angular momentum from the system.

As shown in Section 3.1, at variance to 'wide' interacting systems, the post-flash evolution of IDD is affected by the prompt mass loss, which limits the lifetime and extension of the flash-driven convective shell, thus limiting the feeding of the He-burning shell by convection and reducing the total amount of nuclear energy released during the flash. Such an occurrence prevents the efficient heating of the pre-existing He-rich layers below the He-burning shell and causes the rapid extinction of nuclear burning. Hence, in the post-RLOF phase the accretors in IDD contract very rapidly in order to maintain the thermal equilibrium.

According to the accepted paradigm for the evolution of outbursting binaries, the matter overflowing the accretor Roche lobe leaves the system, taking away the specific angular momentum of the accretor. As a result, the system becomes detached, mass transfer comes to a halt and the WD cools. Hence, the possibility of resumption of nuclear activity depends on the duration of this 'hibernation' phase and the masses of the two components which, in turn, determines the value of $\dot{M}$ at the resumption of mass transfer. As it has been found for the sequence S062+017 (Section 3.1), for an ever decreasing $\dot{M}$, it is possible that the release of gravitational energy occurs in a so long time-scale that it cannot counterbalance the cooling by inward thermal diffusion and neutrino emission and another flash cannot be ignited. For the other systems considered in the present work, this limits the total number of flashes experienced by a given system.

The rough comparison of the present study and Paper I suggests that the expected number of nuclear flashes in IDD is a factor of ~2 lower than the one expected by interpolating the results based on models with constant $\dot{M}$. This reduces further the estimation

obtained in Paper I of only several thousand 'nuclearly active' IDD currently present in the Galaxy.

The results obtained in the current work exhibit a very mild dependence on the initial thermal content of the accretor for cooling ages in the range 0.8–2 Gyr (see Section 3.4), so that they can be considered as representative of the entire population of IDD.

For each fixed initial CO WD mass, as the mass-transfer rate is permanently decreasing, the last flash experienced by accreting WDs is the strongest one (see Figs 9, 10 and 12). As mentioned before, Bildsten et al. (2007) suggested that in a series of flashes the last one may be of dynamical nature (SNe .Ia). None of the systems considered in the present work develops the physical conditions suitable for such a dynamical flash. In particular, we found that the mass of the He-buffer at the onset of the last He-flash is always lower than the critical value necessary to obtain an SNe .Ia, derived by Bildsten and his coauthors for the same WD mass (see fig. 2 in Bildsten et al. 2007 and fig. 1 in Shen & Bildsten 2009). Such a difference has to be ascribed to the different thermal content of the layer below the He-burning shell at the onset of the last He-flash. In our model, the previous accretion history determines the partial heating of the most external zone of the CO WD and of the He-burning shell, so that at the beginning of the last mass-transfer episode driving to an He-flash we have $T_{He} \sim 10^8$ K for both S092+015 and S102+020 systems. As a consequence the 'last flash' in our computations will never attain physical conditions suitable to synthesize iron peak elements. Thus, all three considered systems have the same fate: transformation of the accretor into a massive degenerate object with a CO-core, which has almost the same mass as the initial accretor, and a massive He-buffer, representing a large part of the initial donor.

Recently, Brooks et al. (2015) performed an analysis similar to that of ours , but focused on AM CVn systems with a non-degenerate He-burning star as a donor. Their results cannot be compared directly with our findings because the response to mass extraction of an He-star is different from that of a degenerate object and, hence, the resulting evolution of the host binary system has to be different. Brooks et al. (2015) found that the last He-flash experienced by the accretor of the 'He-star family' of AM CVn systems is never strong enough to produce an SNe .Ia event. So, by combining their results with our results, we can conclude that AM CVn family at large will never produce an explosive event at the end of their life. We remark also that we follow in detail the thermal evolution of the accretors during each flash episode, determining the effective accumulation efficiency, while Brooks et al. (2015) remove the entire He-envelope above the He-burning shell at the onset of the thermonuclear runaway.

Brooks et al. (2015) claim that the first He-flash experienced by AM CVn systems with non-degenerate donors more massive than $0.4M_\odot$ and accretors more massive than $0.8M_\odot$ is 'vigorous enough to trigger a detonation in the helium layer', which could produce either an SNe .Ia or a real Type Ia supernova, if also the CO core detonates. Interestingly enough, this first explosive event could destroy the host binary, thus reducing the expected number of AM CVn systems from this evolutionary channel. This could help in solving the problem of the apparent deficiency of observed AM CVn stars (Carter et al. 2013a). At variance, we find that the first He-flash occurring in the IDD explored in the present study never develops the physical conditions suitable for a detonation in the accreted He-rich buffer. This difference reflects the different behaviour of the mass-transfer rate before the onset of the He-flash: in particular, for IDD $\dot{M}$ is continuously decreasing in time, while it is rising in the binaries studied by Brooks et al. (2015). In this

regard, it is worth noticing that Brooks et al. (2015) consider AM CVn systems with He-stars unevolved or only slightly evolved at the onset of the RLOF. However, the mass-transfer history from He-stars depends on the extent of the donor evolution prior to the RLOF. As a matter of fact the $\dot{M}$ curve may be rising, almost flat or very slightly decreasing (Yungelson 2008).

We recall that in our computation we model the He-WD donor as a zero-temperature object, i.e. as a completely degenerate one. In the real world, however, the most external layers of WDs, independently of their chemical composition, are only partially degenerate or not degenerate at all. As a consequence, when they fill their Roche lobes, the mass-transfer rate increases in time, as it occurs for homogeneous He-star. Once these surface layers have been lost, and the fully degenerate inner region starts to be removed, $\dot{M}$ decreases (Deloye et al. 2007, see also fig. 13 in Paper I). The duration of the first phase of mass transfer depends mainly on the mass of the non-degenerate layers and, in turn, on the cooling age of the donor. On a general ground, such an occurrence implies that the compressional heating of the accretor should occur, at least at the beginning, in a longer time-scale, so that the resulting He-buffer at the onset of the He-flash should be larger. In order to evaluate quantitatively the effect of this rising phase of the mass-transfer rate, we computed several additional models for the S092+015 system by adopting as mass accretion rate:

$$\dot{M} = \min\left(\dot{M}_{FD}, \dot{M}_{FD}^0 \cdot \log\left(1 - \frac{t}{\tau}\right)^{-1}\right), \qquad (3)$$

where $\dot{M}_{FD}$ is the rate derived with the $M - R$ approximation described in Section 2. In the second term, the mass of the partially degenerate/not degenerate layers ΔM_{ND} is parametrized by means of the time-scale τ: large values of τ correspond to large ΔM_{ND}. $\dot{M}_{FD}^0 \simeq 4.978 \times 10^{-7}$ $M_\odot$ yr^{-1} is the value of $\dot{M}_{FD}$ at the onset of the mass transfer. In Fig. 13 we report as a function of the mass transferred from the donor the evolution of the mass-transfer rate described by equation (3), for different values of τ. This figure discloses that for realistic values of $\Delta M_{ND} \leq 0.03$ $M_\odot$, corresponding to $\tau \leq 2$ Myr, ΔM_{tran} increases up to a factor of ~ 3, so that the resulting He-flash is stronger than the one in the S092+015. In any case, we do not expect that this could significantly alter the following evolution, because, as discussed in Section 3.1, the prompt occurrence of the RLOF limits the heating of the He-buffer and, hence, the effects on the thermal properties of the accretor. Values of $\Delta M_{ND} \geq 0.05 M_\odot$, corresponding to $\tau > 5$ Myr, are rather unlikely. According to the results of these numerical experiments, we can conclude that a dynamical event could hardly arise in IDD.

Helium WDs with masses in the range explored in the present study have non-degenerate outer hydrogen layers with mass ≤ 0.01 $M_\odot$ at an age of ~ 1Gyr (Panei et al. 2007), which is usually considered as the typical formation time of AM CVn stars. Transfer of this matter on to the companion upon RLOF may cause explosive phenomena similar to Classical Novae, like in ordinary cataclysmic variables. Recently, Shen (2015) suggested that the ejected matter forms a common envelope in which the components may merge. However, to drive a firm conclusion, it is necessary to consider the interaction of the ejecta with the two components, having in mind, of course, the compactness of the system. This problem, perhaps, demands 3D hydrodynamical simulations.

Strong flashes occurring in the AM CVn systems considered in the present study almost definitely cannot be identified with unique Helium Nova V445 Pup (Ashok & Banerjee 2003; Ashok 2005),
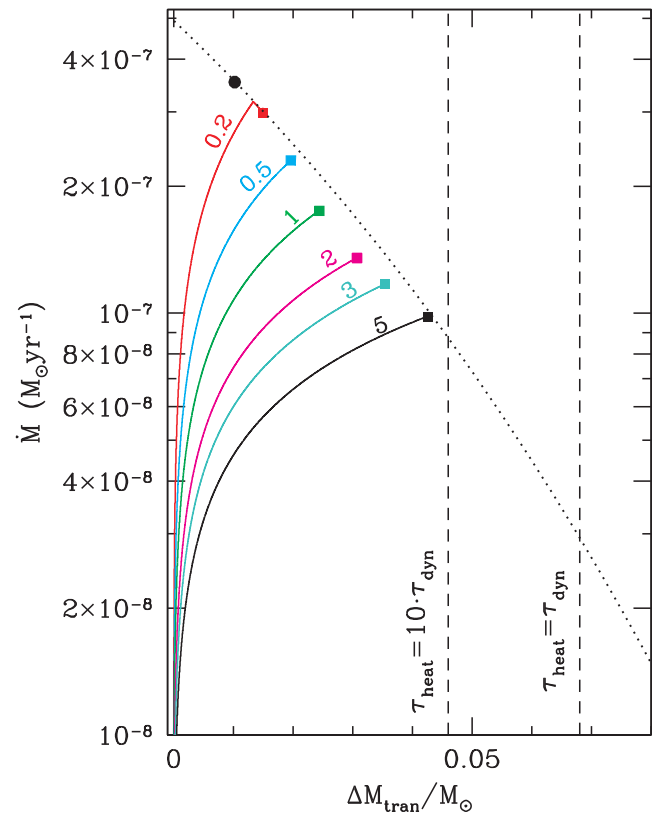

Figure 13. Mass-transfer rate in the S092+015 system as a function of the mass transferred from the donor ΔM_{tran} in different time-scales τ (in Myr), as labelled (solid lines). The dashed line represents accretion rate $\dot{M}_{FD}$ corresponding to fully conservative mass transfer. Filled circle marks the coordinate ($\Delta M_{tran}, \dot{M}$) at the onset of the thermonuclear runaway for the S092+015 system under 'standard' assumptions. Filled squares represent the same quantities for the models computed with different τ. The two vertical lines mark the critical mass of the He-buffer for a 0.92$M_\odot$ CO WD corresponding to the condition $\tau_{heat} = 10\tau_{dyn}$ (left) and $\tau_{heat} = \tau_{dyn}$ (right) as derived from Brooks et al. (2015).

since pre-outburst luminosity of the latter $\log(L/L_\odot) = 4.34 \pm 0.36$ (Woudt et al. 2009) is too high for pre-flash CO WD in IDD. Rather, its progenitor may be a massive (~ 1 $M_\odot$) WD accreting at a rate $\sim 10^{-6}$ $M_\odot$ yr^{-1} from a massive (also ~ 1 $M_\odot$) He-star companion (Woudt et al. 2009; Paper I). A possible progenitor may be similar to the unique sdO+WD system HD 49798 (Mereghetti et al. 2009) with both unusually massive components.

ACKNOWLEDGEMENTS

REFERENCES

Amaro-Seoane P. et al., 2013, GW Notes, 6, 4

Ashok N. M., 2005, Bull. Astron. Soc. India, 33, 75

Ashok N. M., Banerjee D. P. K., 2003, A&A, 409, 1007

Bildsten L., Shen K. J., Weinberg N. N., Nelemans G., 2007, ApJ, 662, L95

Breedt E., Gänsicke B. T., Marsh T. R., Steeghs D., Drake A. J., Copperwheat C. M., 2012, MNRAS, 425, 2548

Brooks J., Bildsten L., Marchant P., Paxton B., 2015, ApJ, 807, 74

Brown W. R., Kilic M., Allende Prieto C., Gianninas A., Kenyon S. J., 2013, ApJ, 769, 66

Cannizzo J. K., Nelemans G., 2015, ApJ, 803, 19

Carter P. J. et al., 2013a, MNRAS, 429, 2143

Carter P. J. et al., 2013b, MNRAS, 431, 372

Chieffi A., Straniero O., 1989, ApJS, 71, 47

D'Antona F., Ventura P., Burderi L., Teodorescu A., 2006, ApJ, 653, 1429

Deloye C. J., Bildsten L., 2003, ApJ, 598, 1217

Deloye C. J., Taam R. E., Winisdoerffer C., Chabrier G., 2007, MNRAS, 381, 525

Drout M. R. et al., 2013, ApJ, 774, 58

Garnavich P., Littlefield C., Terndrup D., Adams S., 2014, Astron. Telegram, 6287, 1

Gehron K., Nagel T., Rauch T., Werner K., 2014, A&A, 562, A132

Han Z., Webbink R. F., 1999, A&A, 349, L17

Kaplan D. L., Bildsten L., Steinfadt J. D. R., 2012, ApJ, 758, 64

Kaplan D. L. et al., 2014, ApJ, 780, 167

Kato T., Hambsch F.-J., Monard B., 2015, PASJ, 67, L2

Kilic M. et al., 2014, MNRAS, 438, L26

Kotko I., Lasota J.-P., Dubus G., Hameury J.-M., 2012, A&A, 544, A13

Krausz D., Nagel T., Rauch T., Werner K., 2010, in Werner K., Rauch T., eds, AIP Conf. Ser. Vol. 1273, XVII European White Dwarf Workshop. Am. Inst. Phys., New York, p. 305

Kremer K., Sepinsky J., Kalogera V., 2015, ApJ, 806, 76

Kulkarni S. R., van Kerkwijk M. H., 2010, ApJ, 719, 1123

Kupfer T. et al., 2015, A&A, 576, A44

Levitan D., Groot P. J., Prince T. A., Kulkarni S. R., Laher R., Ofek E. O., Sesar B., Surace J., 2015, MNRAS, 446, 391

Littlefield C. et al., 2013, AJ, 145, 145

Marsh T. R., Nelemans G., Steeghs D., 2004, MNRAS, 350, 113

Marsh T. R., Gänsicke B. T., Steeghs D., Southworth J., Koester D., Harris V., Merry L., 2011, ApJ, 736, 95

Mereghetti S., Tiengo A., Esposito P., La Palombara N., Israel G. L., Stella L., 2009, Science, 325, 1222

Nelemans G., 2005, in Hameury J.-M., Lasota J.-P., eds, ASP Conf. Ser. Vol. 330, The Astrophysics of Cataclysmic Variables and Related Objects. Astron. Soc. Pac., San Francisco, p. 27

Nelemans G., 2009, Class. Quantum Grav., 26, 094030

Nelemans G., Portegies Zwart S. F., Verbunt F., Yungelson L. R., 2001, A&A, 368, 939

Nomoto K., 1982, ApJ, 253, 798

Panei J. A., Althaus L. G., Chen X., Han Z., 2007, MNRAS, 382, 779

Piersanti L., Tornambé A., Yungelson L. R., 2014, MNRAS, 445, 3239 (Paper I)

Postnov K. A., Yungelson L. R., 2014, Living Rev. Relativ., 17, 3

Ramsay G. et al., 2014, MNRAS, 438, 789

Ruiter A. J., Belczynski K., Benacquista M., Larson S. L., Williams G., 2010, ApJ, 717, 1006

Sepinsky J. F., Kalogera V., 2014, ApJ, 785, 157

Shen K. J., 2015, ApJ, 805, L6

Shen K. J., Bildsten L., 2009, ApJ, 699, 1365

Shen K. J., Guillochon J., Foley R. J., 2013, ApJ, 770, L35

Solheim J., 2010, PASP, 122, 1133

Tutukov A. V., Yungelson L. R., 1979, Acta Astron., 29, 665

Tutukov A. V., Yungelson L. R., 1996, MNRAS, 280, 1035

Verbunt F., Rappaport S., 1988, ApJ, 332, 193

Wagner R. M. et al., 2014, Astron. Telegram, 6669, 1

Warner B., 2003, Cataclysmic Variable Stars. Cambridge Univ. Press, Cambridge

Woudt P. A. et al., 2009, ApJ, 706, 738

Yoon S.-C., Langer N., 2004, A&A, 419, 645

Yungelson L. R., 2008, Astron. Lett., 34, 620

This paper has been typeset from a TEX/LATEX file prepared by the author.